ACTA IMEKO
ISSN: 2221-870X
*September 2023, Volume 12, Number 3, 1 - **7***

Phasor measurement unit based reliability index for renewable-based power systems

Guglielmo Frigo[1], Federica Costa[1], Federico Grasso Toro[1]

[1] *Swiss Federal Institute of Metrology METAS, Lindenweg 50, 3003 Bern-Wabern, Switzerland*

ABSTRACT
The fast growing of renewable energy sources is threatening the correct functioning of power systems, both at the transmission and distribution levels where the presence of converter-interfaced generation (CIG) is rapidly increasing.
Phasor Measurement Units (PMUs) are widely known devices that can enhance power systems observability; however, their in-field performances are still compromised for what concerns low-inertia and fast transient conditions produced by contingencies.
This paper presents a new metric that is able to quantify the discrepancy between the acquired signal and the reconstruction based on the PMU estimates. More specifically, the correspondence between this metric and one of the PMU settings, namely the reporting rate, is examined. This study is carried out in four different scenarios all characterized by a strong presence of distributed CIG, installed at either distribution or transmission levels.
The results indicate the significance of evaluating not only such quantity for correct control but also the importance of the choice of the PMU settings in order to maintain proper control.

Section: RESEARCH PAPER

Keywords: Phasor measurement unit; reliability index; converter-interfaced generation; reporting rate

Citation: Thomas Bruns, Dirk Röske, Paul P. L. Regtien, Francisco Alegria , Template for an Acta IMEKO paper, Acta IMEKO, vol. A, no. B, article C, Month Year, identifier: IMEKO-ACTA-A (Year)-B-C

Section Editor: Section Editor

Received January 1, 2021; **In final form** January 31, 2021; **Published** March 2021

Funding: This work was supported by the Swiss Federal Office of Energy through the QUINPORTION Research Program under Grant SI/502415.

Corresponding author: Guglielmo Frigo, e-mail: guglielmo.frigo@metas.ch

1. INTRODUCTION

Modern power systems are characterized by an ever-increasing penetration of renewable energy sources (RES) and distributed generation (DG). These resources are typically operated in DC and thus require dedicated power converters for a full interconnection with the AC grid [1]. This new paradigm promises to improve grid efficiency by increasing the proximity and the correlation between power generation and consumption [2]. On the other hand, though, it still poses unresolved challenges from the operational point of view [3]. First, many RES rely on natural phenomena (e.g., solar irradiance, wind speed) that are inherently volatile and non-controllable. Second, the so-called Converter-Interfaced Generation (CIG) is not based on big rotating machines and does not contribute to the grid inertia [4]. As a consequence, the grid is more likely to be subject to fast dynamics and transients, as proven by the recent contingencies in South Australia and California [5], [6].

In this context, also the monitoring and control infrastructure shall be accordingly upgraded. The recent literature has investigated the use of Phasor Measurement Units (PMUs) for tracking the evolution of voltage and current signals in the most relevant grid nodes. Indeed, PMUs are capable of providing time-stamped measurements of the phasor, frequency, and rate-of-change-of-frequency (ROCOF) associated with the fundamental component of the power signal. Additionally, by suitably aggregating and comparing measurement from different nodes, it is possible to perform insightful routines like state estimation [7] or fault locations [8].

In this regard, since in our work we are going to focus on the effects of the reporting rate and time latency of PMUs, more details are provided about these aspects.

Specifically, in order to reduce the time latency, there already exists several algorithms illustrated in the literature which are able to compute the estimated synchrophasor over an observation window of two or less cycles of the power system rated frequency [9], [10]. However, the main issue relies on finding a good trade-off between computational speed and accuracy. In this work, the

focus is on power system events occurring at transmission level, therefore the bottleneck relies on the different sources of the algorithm which are characterized by longer timing, such as SCADA systems which may require up to hundreds of seconds.

Not only is the reduction of the latency of utmost importance, but the estimation of power system frequency in real-time is of particular interest. For instance, [11] and [12] illustrate how to perform accurate frequency measurements and how to track its variations in real-time. Indeed, real-time estimation of the power system frequency is a topic of particular interest for both transmission and distribution operators [13]. Having a stream of actual frequency estimates transmitted at a high reporting rate would be extremely useful and practical as this would allow an easy and quick comparison with time-stamped measurements obtained by PMUs. As a matter of fact, it is expected a merge between these two sources of information in the future. Having said that, the objective of our work does not consist in enhancing the performances of PMU devices in terms of sampling frequency, but rather in presenting a new online metric that is able to quantify the discrepancy between the acquired signal and the reconstruction based on the PMU estimates. More in detail, the correspondence between this metric and one of the PMU settings, which is the reporting rate in our case, is examined. In normal operating conditions, the use of PMUs is more frequent given that their accuracy is defined by an international reference standard which is the IEC/IEEE 60255-118-1 (PMU Std) [14]. However, for what concerns frequency measurements, an additional Standard is under development, which is IEC TS 62786-41 detailing the requirements for measurements used to control DER and loads.

Additionally, not only does the PMU Std define the PMU requirements in terms of measurement errors, response time, and reporting latency, but it also introduces two performance classes, i.e., M- and P-class for measurement and protection applications, respectively. The first one is intended for high accuracy, whereas the second one maximizes responsiveness. However, it should be noticed that the PMU Std has been conceived for a "traditional" transmission network scenario, characterized by large inertia and relatively slow variations. As a consequence, some of its performance targets may result to be insufficient or inappropriate for a reduced inertia scenario [15], [16].

The recent experience with grid contingencies has shown that a prompt response (e.g., breaker opening, or load shedding) is crucial for guaranteeing the continuity of operation. Therefore, new PMUs are required to provide optimal performance not only in quasi-stationary conditions but also during the presence of wide-band spectrum events [17]. From a metrological point of view, this represents a critical point as most PMUs rely on static and narrow-band signal models. Indeed, based on these considerations, the PMU Std suspends some of the accuracy requirements during parameter step changes or fast variations (e.g., amplitude or phase modulations).

Another critical aspect is represented by the fact that the PMU performance can be fully characterized in laboratory-controlled conditions, but no information is retrievable on their accuracy in the field [18]. A possible solution in this sense is provided by state estimators that might be able to identify outliers and re-compute the most likely measurement values, based on a set of other PMUs. However, this approach is performed off-line and may fail in the presence of multiple PMUs producing outliers. An alternative solution is represented by locally-computed on-line performance metrics, as the Goodness-of-Fit (GoF) and the normalized Root Mean Squared Error (nRMSE) [19], [20].

These metrics quantify the discrepancy between the acquired signal and the reconstruction based on the PMU estimates. In this way, they determine a sort of definitional uncertainty: the lower the metric, the higher the correlation between the acquired signal and the measurand signal model, and thus the higher the reliability of the PMU measurements.

In previous papers, we investigated the actual metrological significance of these metrics by evaluating their sensitivity against different kinds of disturbances (e.g., wide-band noise, harmonics, fast dynamics) [21]. We discussed their integration into state estimation routines, as a sort of on-line assessment of the weight to associate with each measurement [20]. We also proposed an amendment to the standard composition of the PMU data packet in order to include the metric without significantly affecting the transmission throughput or latency [22].

By extending the preliminary analysis, in this paper, we consider the relationship between these metrics and the PMU settings, namely the reporting rate. In fact, this parameter is known to affect the PMU band-pass filter and responsiveness and it is interesting to see whether similar considerations hold also for the on-line metrics [23].

The paper is organized as follows. Section 2 illustrates the theoretical background, involving both the developed online metric and the PMU model. Section 3 presents four realistic scenarios that are all characterized by the presence of CIG. In this context, the dependence between nRMSE and PMU reporting rate is assessed. Lastly, Section 5 draws some conclusions of this work.

2. THEORETICAL BACKGROUND AND RELIABILITY INDEX

In power systems, a generic voltage or current signal can be represented by the following non-linear dynamic model:

$$x(t) = A \cdot \left(1 + \varepsilon_A(t)\right) \cdot \cos\left(2\,\pi\, f\, t + \varphi + \varepsilon_\varphi(t)\right), \tag{1}$$

where A, f, and φ indicate the amplitude, frequency, and initial phase of the fundamental component, ε_A and ε_φ account for amplitude and phase dynamics (with sinusoidal, linear, or quadratic trends), while t is the time variable.

In real-world conditions, it is reasonable to expect that the signal at the PMU input consists of three components:

$$y(t) = x(t) + \eta(t) + \zeta(t), \tag{2}$$

where η models the narrow-band distortions, namely harmonic and inter-harmonic terms, whereas ζ accounts for wide-band contributions (e.g., uncorrelated Gaussian noise, decaying DC trends or transients).

At first, the PMU acquires the input signal at a constant sampling rate F_s (locked to the UTC time reference):

$$y[n] = y(t = n\,T_s), \quad n = 0, \dots, N_s, \quad T_s = F_s^{-1}, \tag{3}$$

where N_s is the length of the sample series and T_s is the sampling period.

For each sample series, the PMU produces an estimate of the three quantities of interest, namely phasor, frequency, and ROCOF associated to the fundamental component. In the following, the superscript $\hat{}$ indicates the estimated quantities:

$$\hat{f}(t) = \frac{d\hat{\varphi}(t)}{dt}, \quad \widehat{R_f} = \frac{d\hat{\varphi}(t)^2}{dt^2}$$
$$\hat{p} = \hat{A} \cdot \exp\left(1j \cdot \left(2\,\pi\left(\hat{f} - f_0\right) t + \hat{\varphi}\right)\right), \tag{4}$$

where f_0 denotes the system rate frequency (typically, 50 or 60 Hz) and allows for expressing the rotating phase contribution in the presence of off-nominal conditions.

2.1. On-line metric

Among the several on-line metrics for reliability assessment, in this paper we focus on the $nRMSE$, as it is characterized by reduced computational costs and straightforward interpretation. Nevertheless, similar results could be obtained for GoF and other comparable metrics.

Based on the PMU estimates in (4), we can reconstruct the equivalent time-domain trend of the input signal:

$$\hat{y}[n] = \hat{A} \cdot \cos\left(2\,\pi\,\hat{f}\,n\,T_s + \hat{\varphi} + \pi\,\widehat{R_f}\,(n\,T_s)^2\right). \tag{5}$$

The $nRMSE$ is then defined as the squared root of the squared residuals between the reconstructed and the acquired signal:

$$nRMSE = \frac{\sqrt{\sum_n (\hat{y}[n] - y[n])^2}}{N_s}, \tag{6}$$

where the normalization by the sample length N_s is intended for a fairer comparison between different observation intervals. When different nodes' $nRMSE$ values are compared, it might be useful to normalize the metric also by the nominal voltage or current value and express it in per unit.

From a metrological point of view, the $nRMSE$ can be interpreted as the energy discrepancy between the actual acquired signal and what is captured by the PMU. In this context, it is important to observe that the PMU Std adopts a signal model appropriate for narrow-band components centred around the nominal system rate. In the presence of continuous spectrum events, the PMU measurement chain is equivalent to a bandpass filter and the $nRMSE$ accounts for the energy neglected or misrepresented by the phasor formulation. In this sense, the $nRMSE$ is a sort of index of definitional uncertainty due to an inappropriate or simplistic definition of the measurand.

From an operative point of view, it is interesting to observe that the $nRMSE$ has a limited impact on the overall computational complexity. Previous analysis on non-real-time processors have proven how the $nRMSE$ computation time is nearly two orders of magnitude lower than the PMU estimation itself. It is thus reasonable to consider it as a negligible contribution to the overall reporting latency.

2.2. PMU model

The computation of $nRMSE$ is strongly dependent on the considered PMU. A PMU with scarce performance is likely to produce high $nRMSE$ also in operating conditions just slightly deviation from nominal ones. For this reason, in this paper we consider a PMU software model that has been proven to be compliant with both M- and P-class and to perform satisfactorily also in real-world challenging conditions.

In particular, we select the Compressive Sensing Taylor-Fourier Multifrequency (CS-TFM) model because of two main reasons [24]. First, the CS-TFM PMU relies on a dynamic signal model: by means of a Taylor expansion around the reporting time instant, the state variables are not limited to the rotating phasor magnitude and phase, but also to their first- and second-order derivatives. In this way, it is possible to define the fundamental frequency and ROCOF as the instantaneous derivative of phase angle, instead of using finite derivative approximation that inherently introduce low-pass filtering effects and delays. Second, the CS-TFM PMU can be seen as a bank of Taylor-Fourier filters. If properly centred around the signal component frequencies (both informative and spurious), they allow to get a quite wide band-pass filter around the fundamental component, while rejecting the undesired injections of harmonics and inter-harmonics.

In this paper, we reproduce the same CS-TFM implementation originally proposed in [24]. In more detail, we consider the P-class configuration with sampling rate equal to 18 kHz and observation window of three-cycle of the nominal fundamental frequency. These settings are representative of plausible PMU-based protection applications corresponding to 60 or 50 ms for the test scenarios having a 50 or 60 Hz rated power system frequency, respectively. If properly optimized in a real-time controller, the sample series processing requires less than 20 μs. Since the CS-TFM PMU refers its measurements to the observation interval midpoint, it is thus reasonable to say that the reporting latency can be approximated to 30 ms, plus the communication latency that depends on the specific network configuration. Taking as reference the PMU Std compliance tests, the CS-TFM PMU has a worst-case response time of 56.4 ms in the presence of amplitude and phase steps, and a worst-case frequency and ROCOF error of 3.88 mHz and 189 mHz/s, respectively (harmonic distortion test).

Based on these results, it is reasonable to say that the CSTFM PMU represents a viable candidate for PMU applications in reduced-inertia scenarios.

3. SIMULATED SCENARIOS

This Section illustrates four power system test cases, both at transmission and at distribution levels, all characterized by the presence of distributed CIG. The simulated scenarios are inspired by real-world contingencies and well-known benchmark grids. In the following, the simulation details are provided, and the introduced modifications are discussed and motivated.

3.1. South Australia blackout

The first scenario taken into consideration is the well-known South Australia blackout that occurred on September 28th, 2016 [6]. Before the contingency, most of the generating power in the area was based on renewables, in particular wind turbines. Due to extreme weather conditions, the trip of 3 transmission lines initiated a sequence of cascaded faults. At the same time, a protection mechanism caused 9 wind farms to a sustained generation reduction. As a consequence, the South Australia region was suddenly separated from the rest of the system and the frequency started to collapse with an average ROCOF of -6.25 Hz/s. In less than 1 s, the remaining generation facilities were tripped causing the blackout for the entire region. In this paper, we consider a signal portion of 1.2 s where the contingency starts at $t = 3.75$ s.

3.2. Modified IEEE 39-bus system

The second scenario considers a modified version of the IEEE 39-bus system. As further discussed in [25], 4 synchronous machines were replaced by wind turbines having equivalent rated power but characterized by a null contribution to the overall

system inertia, with the aim of replicating inertia-less generation units. Moreover, the traditional static loads were replaced by the EPRI LOADSYN model to account for a more realistic load frequency and voltage responses. Finally, an Under-Frequency Load Shedding (UFLS) routine was implemented in each bus, based on PMU measurements of frequency and ROCOF. Among the different simulated contingencies, in this paper we consider the case of a power loss of 1.5 GW. The test waveform consists of 1.5 s: the generators are tripped at $t = 0.15$ s, this initiate damped oscillations lasting for nearly 0.6 s, and the UFLS begins around $t = 0.8$ s. In this way, it is possible to investigate the $nRMSE$ evolution in three different operating conditions (each one characterized by different spectral characteristics).

3.3. Reduced-inertia IEEE 14-bus system

For the third scenario, we considered the IEEE 14-bus transmission system in Figure 1, comprising 5 synchronous machines [26]. In this case, we reproduced two possible configurations with high and low inertia, respectively.

The first simulation consists of 5 s, and includes the opening of the two circuit breakers (CBs) connected at Bus 2 and 3, at $t = 1$ s. Despite no reclosing is involved, all the generators can still supply all the loads in the power system. For the sake of brevity, in the following we focus on Bus 2, as it is the most affected by the opening. Nevertheless, similar results could be obtained in other nodes.

The second simulation consists of the same contingency, but the inertia constants of the synchronous machines hosted at Bus 2 and 3 have been halved in order to replicate a low inertia power system. This corresponds roughly to a reduction of −9.33% with respect to the previous rated condition.

3.4. IEEE 13-bus system with PV integration

The final scenario, instead, refers to a distribution grid. More precisely, we consider the well-known IEEE 13-bus test system, but we introduce some substantial changes in order to account for the ever-growing distributed generation also at low-voltage levels [28].

To this purpose, three new buses are added with respect to the original distribution feeder, each of them hosting a single-phase photovoltaic unit (PV) with a rated power of 3.5 kW [29], [30]. In order to introduce a plausible level of harmonic content generated by the PV, we recreate three different irradiance cycles having low levels of irradiance which have been proved to introduce a non-negligible level of harmonics and interharmonics [31]. In more detail, Bus 611.1 is connected to Bus 611 with a 3000 ft line, Bus 652.1 and Bus 652.2 are connected to Bus 652 with a 10000 and 15000 ft lines, respectively. In this feeder, a phase-to-ground fault occurs along the line connecting Bus 684 to Bus 652. Therefore, we focus on Bus 652, highlighted in red in Figure 2. The fault occurs at $t = 2.220$ s, and it is cleared at $t = 2.255$ s. This scenario replicates the typical response of a low-voltage CB, with a clearance time below 3 cycles of nominal system rate.

4. RESULTS AND DISCUSSION

In this Section, we present the results obtained in the four considered scenarios. In particular, we focus on the feasibility of detecting transient or anomalous conditions based on the $nRMSE$ and on the quantification of the latency of the entire measurement process (e.g., acquisition, parameter extraction, $nRMSE$ computation). In order to find the most suitable configuration, we investigate the relationship between the

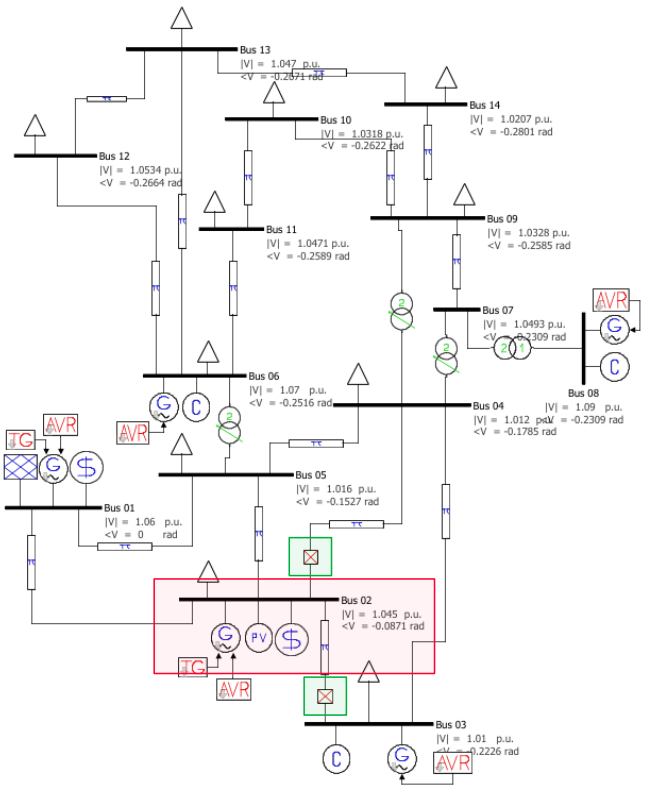

Figure 1. IEEE 14-Bus system in PSAT toolbox [27]: Bus 2 and the two CBs are highlighted in red and green, respectively.

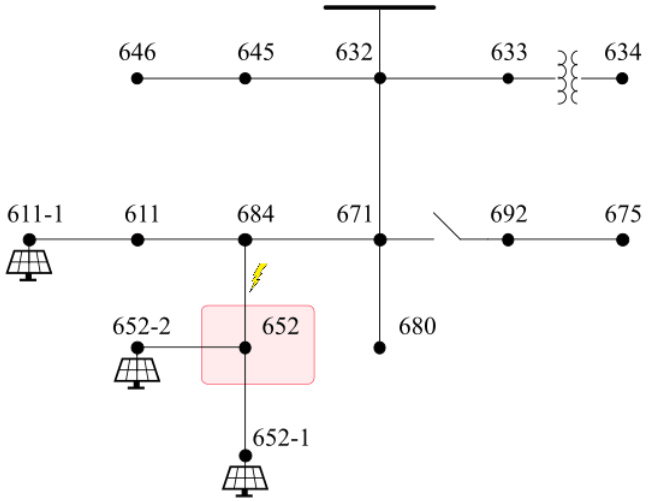

Figure 2. IEEE 13-Bus system highlighting Bus 652 (in red) and fault location (lightning bolt).

$nRMSE$ latency and the PMU reporting rate. For this analysis, we vary the PMU reporting rate spanning over the entire PMU Std range, i.e., from 10 to 100 or 120 frames per second (fps) for 50 and 60 Hz nominal system rate, respectively.

In this paper, we consider the $nRMSE$ as a local index of measurement reliability, relative to a specific node in a specific time instant. Therefore, it is not metrologically relevant to compare $nRMSE$ values taken in different networks and time instants. In fact, the $nRMSE$ is strongly dependent on the uncorrelated noise introduced by the PMU $nRMSE$ front end, that may vary from bus to bus or based on external conditions

Table 1. nRMSE Transient Detection Latency in ms based as Function of PMU Reporting Rate.

R_r (fps)	Scenario		R_r (fps)	Scenario	
	A	B		C	D
10	n.a.	115	10	55	65
25	85	95	30	47	55
50	65	75	60	45	38
120	55	65	120	38	30

(e.g., temperature, satellites' availability, etc.). The idea is to detect a potentially anomalous condition by means of a simple thresholding process. First, we define the expected $nRMSE$ value as the mean value over 0.2 s of normal operating conditions. Then, we detect an anomalous condition as soon as the $nRMSE$ exceeds the expected value by three orders of magnitude.

In the following, we quantify the $nRMSE$ latency as the difference between when the $nRMSE$ has exceeded the threshold (comprising acquisition and processing latency). In Table 1, we report the results obtained for the four considered scenarios (further considerations are provided in the corresponding subsections).

4.1. South Australia blackout

The first scenario reproduces a critical operating condition, where the system collapses to black-out in less than 1 s. In such an unfortunate concatenation of adverse events, it is reasonable to say that even a prompt detection would have not guaranteed the continuity of operation. Nevertheless, the sooner the event is detected, the sooner its mitigation can be initiated.

In this context, Figure 3(a) shows the system frequency as function of time. Starting at t = 3.75 s, a first significant step is noticed. After a reduced attempt of restoration, at t = 3.9 s the frequency begins a stable and steep decrease that will lead to the generation units' trip and the consequent black-out.

In Figure 3(b) we present the corresponding $nRMSE$ values obtained with four different reporting rates, namely $R_r = 10, 25, 50, 100$ fps. In this regard, it is interesting to observe the discrepancy between the initial portion in (quasi) normal operation and the post-contingency evolution. The non-constant trend at the beginning is motivated by the reduced inertia of the network (mostly relying on wind generation), but still the observed fluctuations are not so relevant.

The identification of the contingency occurrence time is strongly dependent on the selected reporting rate. At the minimum reporting rate ($R_r = 10$ fps), the $nRMSE$ peaks related to the two discontinuities in the frequency evolution are not even detected. The $nRMSE$ increases progressively but smoothly according to a nearly linear trend, but never exceeding the threshold. With higher reporting rates, instead, the contingency is correctly detected. The higher the reporting rate, the lower the latency. In particular, with $R_r = 100$ fps, the transient is detected within 55 ms, i.e., less than 3 nominal cycles (comparably with the PMU response time as per the PMU Std test).

4.2. Modified IEEE 39-bus system

The second scenario presents a typical case of system contingency and consequent restoration by means of UFLS. As a consequence, the test waveform in Figure 4(a) can be divided into three consecutive portions. First, a steady-state condition.

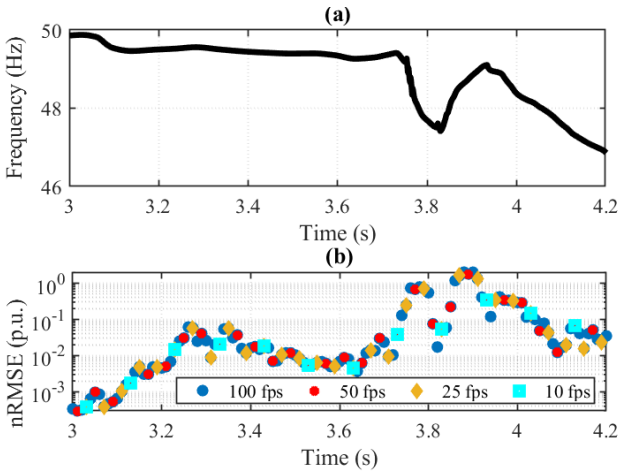

Figure 3. System frequency as function of time (a). Corresponding $nRMSE$ values with different PMU reporting rates (b).

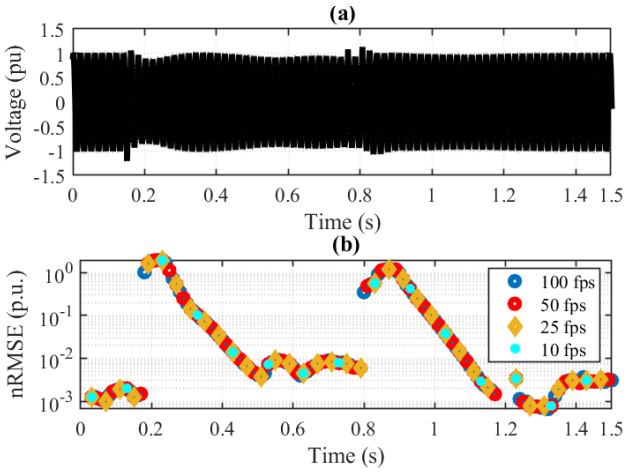

Figure 4. Voltage profile as function of time (a). Corresponding $nRMSE$ values with different PMU reporting rates (b).

Then, the generators' trip and the consequent damped oscillations. Finally, the beginning of the UFLS.

In order to avoid further instabilities, system operators perform UFLS and similar mitigation mechanisms with time scales in the order of hundreds ms. In this context, $nRMSE$ can be used either as contingency detector, but also as an indicator of system stability. Only when damped oscillations have extinguished (and thus the $nRMSE$ has gone back to expected value), it is convenient to undertake a new control action.

In Figure 4(b), we present the corresponding $nRMSE$ values for the considered reporting rates. The transient is detected independently from the selected R_r, but a higher reporting rate allows for nearly halving the detection latency down to 65 ms. Another interesting aspect is represented by the $nRMSE$ capability of tracking the damped oscillation level. After the contingency, it takes nearly 0.25 s to come back to a quasi-stationary condition. A similar trend is visible after the first load shedding (in line with the system operators' guidelines).

4.3. Reduced-inertia IEEE 14-bus system

The third scenario is intended to compare rated and reduced inertia conditions.

Without loss of generality, the following graphs refer only to the maximum reporting rate ($R_r = 120$ fps). For this analysis,

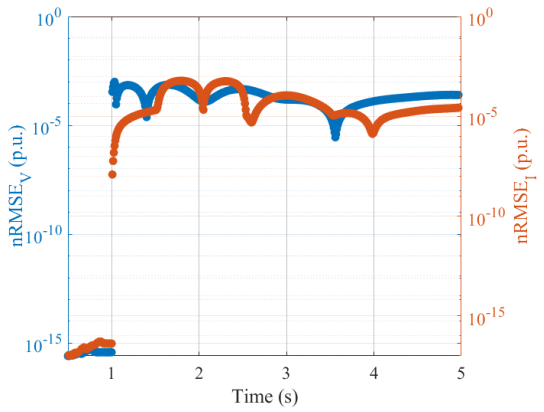

Figure 5. Voltage and current $nRMSE$ measured at Bus 2 with R_r = 120 fps in rated-inertia conditions.

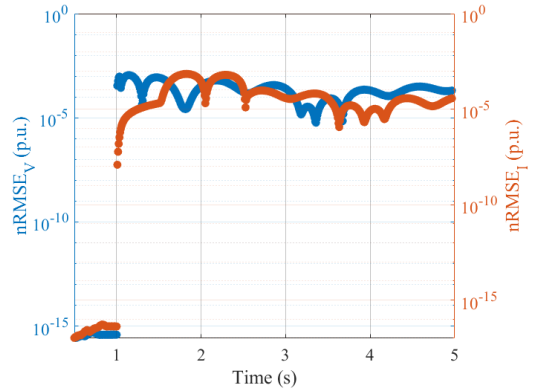

Figure 6. Voltage and current $nRMSE$ measured at Bus 2 with R_r = 120 fps in low-inertia conditions

we consider the $nRMSE$ on both voltage and current signals at Bus 2, since it is the closest to the CB opening. In this regard, Figure 5 and Figure 6 present the $nRMSE$ time evolution in rated and reduced inertia conditions, respectively. In both cases, the CB opening corresponds to a sharp transition in the $nRMSE$ values. Afterwards, the reduction of inertia is evident in the irregular and oscillatory trend.

In terms of latency, all the reporting rates allow for a prompt detection. Therefore, in the presence of CB opening, the use of higher reporting rates implies limited advantages (i.e., a latency reduction of less than 1 nominal cycle).

4.4. IEEE 13-bus system with PV integration

In the last scenario, we consider a CB opening and reclosing after less than three nominal cycles. It is therefore interesting to evaluate the $nRMSE$ response in the presence of two consecutive transients.

In this context, Figure 7 presents the $nRMSE$ profile as computed on the current waveform at Bus 652 for different reporting rates. In particular, the graph focuses on the occurrence of the CB opening and re-closing. The first transition is easily detected with all reporting rates: as in the previous scenario, higher reporting rates produce limited enhancement in terms of detection latency.

On the other hand, with a too low reporting rate ($R_r = 10$ fps) the threshold is exceeded a single time and could be mistaken for an outlier. Conversely, the highest reporting rate ($R_r = 120$ fps) allows for quantifying the contingency duration and accurately tracking the progressive restoration of normal operation.

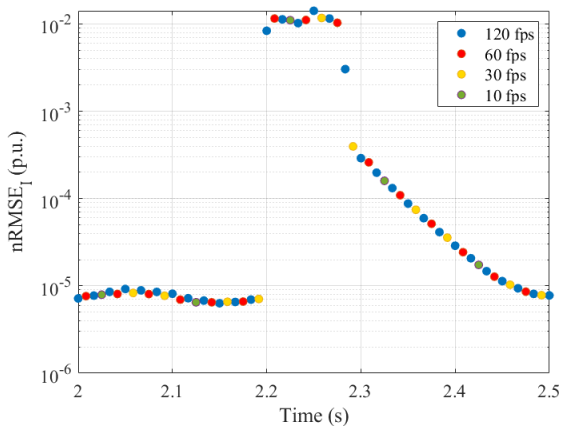

Figure 7. Current $nRMSE$ measured at Bus 652 during the contingency, using all possible R_r for a 60-Hz PMU.

5. CONCLUSIONS

The installation of distributed generation in transmission and distribution systems is resulting in a general decrease in the overall system inertia. In such conditions, low latency is required in order to promptly detect possible contingencies.

PMUs constitute a promising solution in such a scenario, however, in the current state, their performances are unreliable. Therefore, new requirements are necessary for what concerns their performance targets during transient conditions. A possible solution involves the development of an online metric that is able to track power system transients and discern them from normal steady-state operation.

In this paper, we considered the $nRMSE$ as an online reliability index based on PMU measurements. In this work, we have tested the $nRMSE$ in four different realistic scenarios, all characterized by the strong presence of renewable-based generation. More specifically, the dependence between the $nRMSE$ and the PMU reporting rate has been analysed, spanning over the entire set of values provided by the PMU Std.

The results indicate that the higher the reporting rate, the lowest the time latency in the identification of contingencies and possible system oscillations. This outcome is particularly useful not only for the setting of power system protections but also for whether new control actions need to be undertaken.

ACKNOWLEDGEMENT

This work was supported by the Swiss Federal Office of Energy through the QUINPORTION Research Program under Grant SI/502415.

REFERENCES

[1] C. Cecati, C. Citro, P. Siano, Combined operations of renewable energy systems and responsive demand in a smart grid, IEEE Transactions on Sustainable Energy 2(4) (2011), pp. 468–476. DOI: 10.1109/TSTE.2011.2161624

[2] A. J. Ahmed, M. H. Alkhafaji, A. J. Mahdi, Performance enhancement of a low-voltage microgrid by measuring the optimal size and location of distributed generation, Acta IMEKO 11(3) (2022), pp. 1–8. DOI: 10.21014/acta_imeko.v11i3.1270

[3] A. Nikolic, B. Babic, A. Zigic, N. Miladinovic, S. Milosavljevic, Simultaneous power quality analysis of feeders in mv utility power stations, Acta IMEKO 4(1) (2015), pp. 53–60.

DOI: 10.21014/acta_imeko.v4i1.163
[4] M. Paolone, T. Gaunt, X. Guillaud, M. Liserre, S. Meliopoulos, A. Monti, T. Van Cutsem, V. Vittal, C. Vournas, Fundamentals of power systems modelling in the presence of converter-interfaced generation, Electric Power Systems Research 189 (2020), art. No. 106811.
DOI: 10.1016/j.epsr.2020.106811
[5] FERC and NERC, Arizona-Southern California outages on September 8, 2011, causes and recommendations. Online [Accessed 25 August 2023]
http://www.nerc.com/pa/rrm/ea
[6] AEMO, Black system South Australia 28 September 2019 - final report, Online, March 2017. Online [Accessed 25 August 2023]
http://www.aemo.com.au/
[7] A. von Meier, E. Stewart, A. McEachern, M. Andersen, L. Mehrmanesh, Precision micro-synchrophasors for distribution systems: A summary of applications, IEEE Transactions on Smart Grid 8(6) (2017), pp. 2926–2936
DOI: 10.1109/TSG.2017.2720543
[8] M. Pignati, L. Zanni, P. Romano, R. Cherkaoui, M. Paolone, Fault detection and faulted line identification in active distribution networks using synchrophasors-based real-time state estimation, IEEE Transactions on Power Delivery 32(1) (2017) pp. 381–392.
DOI: 10.1109/TPWRD.2016.2545923
[9] G. Frigo, P. A. Pegoraro, S. Toscani, Low-Latency, Three-Phase PMU Algorithms: Review and Performance Comparison, Applied Sciences 11(5) (2021) art. No. 2261.
DOI: 10.3390/app11052261
[10] G. Frigo, A. Derviškadić, M. Paolone, Reduced leakage synchrophasor estimation: Hilbert transform plus interpolated DFT, IEEE Transactions on Instrumentation and Measurement 68(10) (2019), pp. 3468-3483.
DOI: 10.1109/TIM.2018.2879070
[11] A. Radonjic, P. Sovilj, V. Vujicic, Digital Measurement of Power System Frequency using a Two-bit A/D converter.
[12] A. Ghanavati, H. Lev-Ari, A. M. Stanković, A sub-cycle approach to dynamic phasors with application to dynamic power quality metrics, IEEE Transactions on Power Delivery 33(5) (2018), pp. 2217-2225.
DOI: 10.1109/TPWRD.2018.2798923
[13] A. Silverstein, J. Follum, High-Resolution, Time-Synchronized Grid Monitoring Devices, North American Synchrophasor Initiative Technical Report, March 2020.
[14] IEEE/IEC International Standard - Measuring relays and protection equipment - Part 118-1: Synchrophasor for power systems - Measurements, IEC/IEEE 60255-118-1, Dec 2018.
[15] P. Castello, C. Muscas, P. A. Pegoraro, S. Sulis, Low-cost implementation and characterisation of an active phasor data concentrator, Acta IMEKO 8(2) (2019), pp. 21–27.
DOI: 10.21014/acta_imeko.v8i2.625
[16] G. Frigo, A. Derviskadic, Y. Zuo, and M. Paolone, Pmu-based rocof measurements: Uncertainty limits and metrological significance in power system applications, IEEE Transactions on Instrumentation and Measurement 68(10) (2019), pp. 3810–3822.
DOI: 10.1109/TIM.2019.2907756
[17] G. Frigo, A. Derviskadic, P. A. Pegoraro, C. Muscas, M. Paolone, Harmonic phasor measurements in real-world PMU-based acquisitions, 2019 IEEE International Instrumentation and Measurement Technology Conference (I2MTC), Auckland, New Zealand, 20-23 May 2019, pp. 1–6.
DOI: 10.1109/I2MTC.2019.8826988
[18] G. Frigo, A. Derviskadic, D. Colangelo, J. Braun, M. Paolone, Characterization of uncertainty contributions in a high-accuracy PMU validation system, Measurement 146 (2019), pp. 72–86.
DOI: 10.1016/j.measurement.2019.06.013
[19] A. Riepnieks, H. Kirkham, An introduction to goodness of fit for pmu parameter estimation, IEEE Transactions on Power Delivery 32(5) (2017), pp. 2238–2245.
DOI: 10.1109/TPWRD.2016.2616761
[20] G. Frigo, F. Grasso Toro, On-line performance assessment for improved sensor data aggregation in power system metrology, Measurement: Sensors 18 (2021), art. No. 100186.
DOI: 10.1016/j.measen.2021.100186
[21] G. Frigo, F. G. Toro, Metrological significance and reliability of online performance metrics in PMU-based wls state estimation, in 2022 International Conference on Smart Grid Synchronized Measurements and Analytics (SGSMA), Split, Croatia, 24-26 May 2022, pp. 1–6.
DOI: 10.1109/SGSMA51733.2022.9806016
[22] G. Frigo, F. Costa, F. Grasso Toro, PMU-based metrics for power quality assessment in distributed sensor networks, 2022 IMEKO TC-4 International Symposium 1 (2022), pp. 1–6.
DOI: 10.21014/tc4-2022.09
[23] P. Castello, C. Muscas, P. A. Pegoraro, S. Sulis, Monitoring system based on phasor measurement units with variable reporting rates, Acta IMEKO 7(4) (2018), pp. 62–69.
DOI: 10.21014/acta_imeko.v7i4.585
[24] G. Frigo, A. Derviskadic, Y. Zuo, A. Bach, M. Paolone, Taylor-fourier pmu on a real-time simulator: Design, implementation and characterization, 2019 IEEE Milan PowerTech, 2019, Milan, Italy, 23-27 June 2019, pp. 1–6.
DOI: 10.1109/PTC.2019.8810660
[25] Y. Zuo, G. Frigo, A. Derviskadic, M. Paolone, Impact of synchrophasor estimation algorithms in rocof-based under-frequency loadshedding, IEEE Transactions on Power Systems 35(2) (2020), pp. 1305–1316.
DOI: 10.1109/TPWRS.2019.2936277
[26] IEEE, 14 bus power flow test case, online, August 1993. Online. [Accessed 25 August 2023]
http://labs.ece.uw.edu/pstca/pf14/pg_tca14bus.htm
[27] F. Milano, An open-source power system analysis toolbox, IEEE Transactions on Power Systems 20(3) (2005), pp. 1199–1206.
DOI: 10.1109/TPWRS.2005.851911
[28] W. Kersting, Radial distribution test feeders, IEEE Transactions on Power Systems 6(3) (1991), pp. 975–985.
DOI: 10.1109/59.119237
[29] G. Crotti, D. Giordano, Set up and characterization of a measuring system for PQ measurements in a mv site with PV generation, Acta IMEKO 4(1) (2015), pp. 97–104.
DOI: 10.21014/acta_imeko.v4i1.171
[30] G. Bucci, F. Ciancetta, E. Fiorucci, A. Delle Femine, Thermographic and electrical characterisation of a photovoltaic panel under partial shading conditions: a case study, Acta IMEKO 8(1) (2019), pp. 93–102.
DOI: 10.21014/acta_imeko.v8i1.609
[31] R. Langella, A. Testa, J. Meyer, F. Moller, R. Stiegler, S. Z. Djokic, Experimental-based evaluation of PV inverter harmonic and interharmonic distortion due to different operating conditions, IEEE Transactions on Instrumentation and Measurement 65(10) (2016), pp. 2221–2233.
DOI: 10.1109/TIM.2016.2554378